European Conference on Optical Communication (ECOC) 2022 © Optica Publishing Group 2022

1 x 5 Silicon Nitride MEMS Optical Switch

Suraj Sharma(1), Niharika Kohli(2), Michaël Ménard(1), and Frederic Nabki(1)

(1) Department of Electrical Engineering, École de technologie supérieure, Montréal, Québec H3C 1K3, Canada, suraj.sharma.1@ens.etsmtl.ca
(2) CMC Microsystems, 111 Notre-Dame West, Montréal, Québec H3C 6M8, Canada

Abstract *We demonstrate the first 1x5 electrostatic MEMS optical switch with silicon nitride waveguides that combines analog and digital control. It achieves average insertion losses between 2.2 dB and 5.39 dB for the five switching channels and operates over a wavelength range of 85 nm. ©2022 The Author(s)*

Introduction

Photonic switching technology has been proposed to implement access networks based on the next generation passive optical networks 2 (NG-PON2) standard with 4 to 8 switching channels [1]. Conventional silicon nitride (SiN) photonics based optical switching technology is energy inefficient because it relies on the thermal tuning of optical components, such as ring resonators and Mach-Zehnder interferometers, which consumes high power [2,3]. Microelectromechanical systems (MEMS) based optical switching using electrostatic actuation consumes low power and provides broadband operation. Most MEMS based integrated optical switches are based on silicon (Si) photonics [4,5] which complicates design by combining optical and mechanical constraints. SiN waveguides can provide low propagation loss in comparison to Si waveguides and work over a wider wavelength range [6]. However, only a few MEMS based optical switches have been developed with integrated SiN photonics [7,8].

This work is a significant improvement upon our previous device that relied on MEMS based digital switching between SiN waveguides in a 1 x 3 switching configuration [9]. Here, our new MEMS based optical switch demonstrates analog control over three switching positions. The device also provides digital switching between 2 additional channel waveguides completing a 1 x 5 switching configuration. The 85 nm operational wavelength range between 1540 nm and 1625 nm is also an improvement on our previous SiN optical switch demonstration [9].

Operating Principle

Our 1 x 5 optical switch relies upon two electrostatic parallel plate actuators on opposite sides of the platform shown in Fig. 1(a). The left switching (LSW) and right switching (RSW) actuators can displace the platform with suspended waveguides by up to 5 µm with analog control, and by up to 8 µm with digital control in the left and right direction respectively, as per the top view of the device design shown in Fig. 1(a). Mechanical stoppers of 10 µm in length on the opposite sides of each switching actuator prevents device shorting during digital switching, which relies upon the pull-in phenomenon of the electrostatic actuators. The unique single beam spring design anchors the device at two points towards the top of the structure. This cantilever like spring structure allows us to achieve large switching displacement with analog control in comparison to our previous work with the same

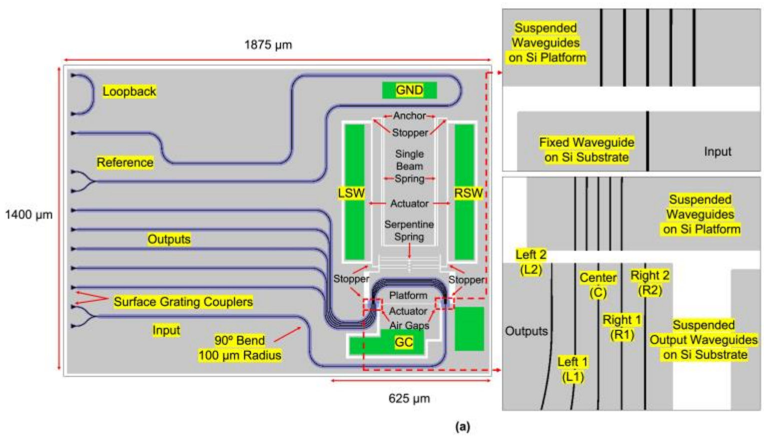

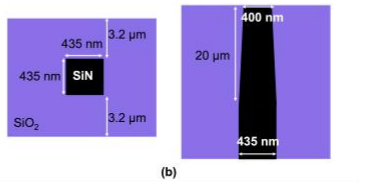

Critical MEMS Parameter		Dimension (µm) Design	Fabricated
Stopper Gap	Left Switching	8	8.43 – 8.56
	Right Switching	8	8.5 – 8.81
	Gap Closing	4	3.42 – 3.51
Actuator Gap	Left Switching	15	16.2 – 16.4
	Right Switching	15	16.2 – 16.4
	Gap Closing	6	7.2 – 7.28
Spring	Single Beam Width	5	4.71 – 4.84
	Serpentine Beam Width	5	4.71 – 4.96

(c)

Fig. 1: (a) Schematic of the 1 x 5 optical switch with zoomed in view of the waveguide interface at the edge of the platform. (b) Cross-sectional view of the SiN waveguides with dimensions, and top view of the inverted tapers used near the edge of the switching platform with dimensions. (c) Design vs fabricated dimensions for critical MEMS parameters.

European Conference on Optical Communication (ECOC) 2022 © Optica Publishing Group 2022

cavity size of 1400 µm by 625 µm [9]. The serpentine spring structure allows the displacement of the platform in the downward direction upon actuation of the gap closing (GC) actuator as per the top view of the device design shown in Fig. 1(a). This actuator relies upon the pull-in phenomenon to digitally close the two air gaps. The GC actuator allows closing the two air gaps between the suspended and fixed waveguides shown in the zoomed in views of the device in Fig. 1(a). The reference waveguide structure (i.e., loopback) shown in Fig. 1(a) is used for the measurement of the coupling losses.

During analog actuation, the input waveguide shown in Fig. 1(a) can be aligned to the center (C), left 1 (L1) or right 1 (R1) switching channel. The LSW and RSW actuators can be used for fine alignment between the suspended and fixed waveguides. Digital actuation after electrostatic pull-in of the switching actuators allows us to align the input waveguide to the left 2 (L2) or right 2 (R2) output waveguides. The GC actuator is used in all switching positions for efficient transmission of the optical signal between input and output waveguide channels. The SiN waveguide core dimensions are 435 nm by 435 nm with 3.2 µm thick top and bottom silicon oxide (SiO_2) claddings as shown in Fig. 1(b). The inverted taper design of waveguide core also shown in Fig. 1(b) near the air gaps minimizes optical loss during switching. The key MEMS parameters along with the designed and fabricated dimensions are presented in Fig. 1(c). The effects of fabrication variations on the different switching positions and the actuation voltage are discussed below.

Microfabrication and Experimental Setup

The 1 x 5 optical switch was fabricated through a proprietary microfabrication process by AEPONYX Inc., which also used to fabricate our previous 1 x 3 optical switch [9]. The layers forming the optical waveguides are grown and patterned over a cavity silicon-on-insulator (CSOI) wafer with a 59 µm thick Si device layer and predefined cavities to facilitate the release of the MEMS. The MEMS are patterned and etched in the device layer after fabrication of the waveguides. Scanning electron microscope (SEM) imaging was used to measure the fabricated dimensions and are shown in Fig. 2(a).

A schematic of the test setup used is shown in Fig. 2(b). The test device was wirebonded to a custom printed circuit board (PCB). The PCB was then placed on a bi-axial stage controlled with a microposition controller that is also used to move the fiber array vertically over the sample for fine alignment. An input optical signal from a T100S-HP laser from EXFO is coupled through the fiber array to the input waveguide using a surface grating coupler (SGC) on the fabricated device. The actuators of the optical switch are connected to two high voltage DC sources as per the test circuit shown in Fig. 1(b). The optical signal is switched between the different output waveguides in all five switching positions during these measurements. We measured the transmission response in all switching positions with and without the GC actuator. Light from the SGCs on the output waveguides couples to the fiber array and is detected with a CT440 optical component tester from EXFO. Polarization maintaining fibers were used to measure the transmission response of different switching positions for the transverse electric (TE) mode only since our SGCs were optimized for this polarization.

Results and Discussion

Fig. 3(a) shows the normalised transmission data in the five switching positions with the GC actuator in ON and OFF state. The optical switch operates in the wavelength range of 1540 nm to 1625 nm. The range is limited by the bandwidth of the SGCs and not by the switch. The fluctuations in the transmission curve come from the SGCs used for optical coupling between the fiber array and the waveguides. The reference

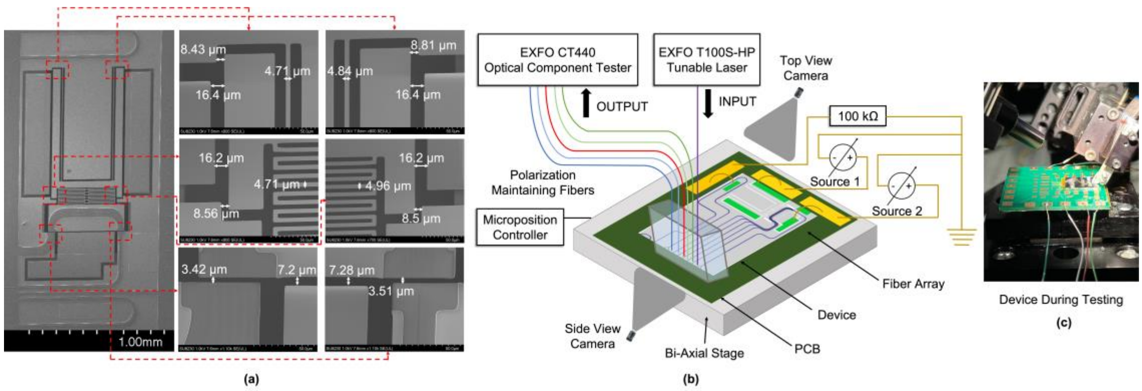

Fig. 2: (a) SEM image of the fabricated 1x5 optical switch. (b) Schematic of the optical characterization test setup with the test circuit used for MEMS actuation with RSW and GC actuators. (c) Wirebonded sample during measurements.

waveguide structure shown earlier in Fig. 1(a) was used for normalization of the transmission data and calculation of the average insertion loss over the wavelength range presented in Fig. 3(a). The average insertion loss in all five switching positions with the GC actuator ON is shown in table 1. The table also compares the results for this device with our previous digitally controlled 1 x 3 SiN optical switch.

Tab. 1: Device Performance Comparison

Switch Type	Average Insertion Loss (dB)				
	L2	L1	C	R1	R2
1x5	5.39	3.38	4.12	2.2	4.13
1x3 [9]	5.35	NA	4.97	NA	6.49

Insertion loss in the three switching positions controlled through analog motion of the switching actuator before electrostatic pull-in allows fine alignment between the suspended and fixed waveguides. Thus, lower losses are observed in the L1, C, and R switching channels compared to other channels. The switching channels at the extremities, L2 and R2, rely on digital control of the switching actuator based on electrostatic pull-in, hence they show similar performance to the 1x3 digital switch in [9]. The alignment between the suspended and fixed waveguides for the L2 and R2 switching positions is limited by the precision in the fabrication of the stopper gap, which can vary from of 430 nm to 881 nm as shown in Fig. 1(c). Therefore, higher optical losses are observed in the two outermost channels.

The lowest average insertion loss (2.2 dB) was obtained for the R1 channel with analog control whereas the maximum average insertion loss was 5.39 dB for the L2 channel with digital control. It should be emphasized that this loss includes two air gaps (although closed), thus the per-gap-loss to about half of this value. The variation in optical loss between channels with analog control could be due to the residual stress variation caused by the waveguide and cladding layers across the suspended platform. Such residual stress can cause out-of-plane misalignment between the waveguides. The average crosstalk in adjacent waveguides for all five switching positions with the GC actuator ON was less than 36 dB. The fine alignment capability of the device is shown in Fig. 3(b) with the impact of variations in voltage on the average insertion loss at different switching positions. The impact of the GC actuator on the optical losses is also shown in Fig. 3(b).

Conclusion

We demonstrated the first 1 x 5 SiN optical switch with analog and digital control through electrostatic MEMS actuation. The novel actuation mechanism allows us to finely align in three switching positions with minimum average insertion loss in the range of 2.2 dB – 4.12 dB. Average insertion loss in the two additional switching positions range between 4.13 dB – 5.39 dB. The demonstrated wavelength range of 85 nm between 1540 nm – 1625 nm is an improvement over our previous optical switch that had a 50 nm operational wavelength range between 1530 nm – 1580 nm [9]. Optimization of the residual stress in the optical layers fabricated over suspended Si platform can improve device performance with minimum loss variation between different switching positions.

Acknowledgement

The authors would like to acknowledge the financial, technical, and microfabrication support of AEPONYX Inc. Financial support was also provided by NSERC, PRIMA Québec and ReSMiQ.

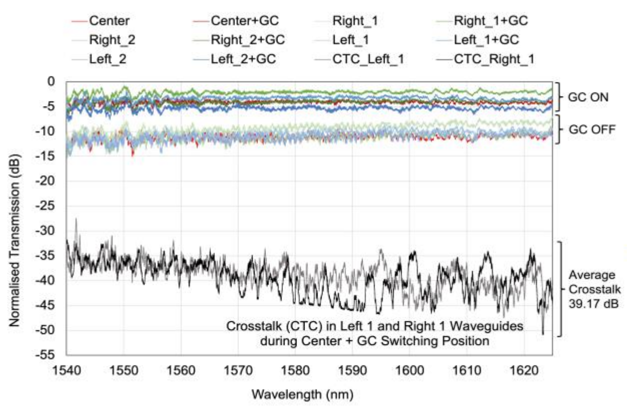

(a)

Switching Channel	Control Type	Actuator Used	Actuation Voltage (V)	Average Insertion Loss (dB)	Average Insertion Loss Reduction With GC Actuator ON (dB)
Left 2 (L2)	Digital	LSW	90	11.19	
			85	10.6	
Left 1 (L1)	Analog	LSW	86	10.51	
			87	10.76	
		LSW	10	11.38	
		LSW	5	11.36	
Center (C)	Analog	None	0	11.5	
		RSW	5	11.11	
		RSW	10	11.16	
			85	9.52	
Right 1 (R1)	Analog	RSW	86	9.25	
			87	9.52	
Right 2 (R2)	Digital	RSW	89	11.16	
Left 2 (L2)	Digital	LSW + GC	90 + 120	5.39	5.8
			82 + 120	4.01	
Left 1 (L1)	Analog	LSW + GC	83 + 120	3.38	7.13
			84 + 120	3.48	
Center (C)	Analog	GC Only	120	5.32	
		LSW + GC	40 + 120	4.12	6.99
			76 + 120	2.61	
Right 1 (R1)	Analog	RSW + GC	77 + 120	2.38	
			78 + 120	2.2	7.05
Right 2 (R2)	Digital	RSW + GC	89 + 120	4.13	7.03

(b)

Fig. 3: (a) Normalised transmission response of the 1x5 optical switch tested in all switching positions with GC actuator in ON and OFF states. (b) Fine alignment capability shown by average insertion loss measurements in the wavelength range of 1540 nm to 1625 nm at different actuation voltages, and average insertion loss reduction with GC actuator in ON state.

References

[1] S. Inoue, S. Nishimura, M. Nakahama, A. Matsutani, T. Sakaguchi, and F. Koyama, “High-speed wavelength switching of tunable MEMS vertical cavity surface emitting laser by ringing suppression,” *Japanese Journal of Applied Physics*, vol. 57, no. 4, pp. 040308, 2018. DOI: https://doi.org/10.7567/JJAP.57.040308

[2] J. Pan, S. Zhai, J. Feng, M. Shi, L. Zhou, G. Cong, R. Akimoto, and H. Zeng, “Double-layer cross-coupled silicon nitride multi-ring resonator systems,” *IEEE Photonics Technology Letters*, vol. 32, no. 5, pp. 227-230, 2020. DOI: 10.1109/LPT.2020.2968291

[3] Z. Yong, H. Chen, X. Luo, A. Govdeli, H. Chua, S. S. Azadeh, A. Stalmashonak, G. Q. Lo, J. K. S. Poon, and W. D. Sacher, "Power-efficient silicon nitride thermo-optic phase shifters for visible light," *Optics Express*, vol. 30, pp. 7225-7237, 2022. DOI: 10.1364/OE.448614

[4] T. J. Seok, N. Quack, S. Han, R. S. Muller, and M. C. Wu, “Highly scalable digital silicon photonic MEMS switches,” *Journal of Lightwave Technology*, vol. 34, no. 2, pp. 365-371, 2015. DOI: 10.1109/JLT.2015.2496321

[5] Y. Akihama, Y. Kanamori, and K. Hane, “Ultra-small silicon waveguide coupler switch using gap-variable mechanism,” *Optics Express*, vol. 19, no. 24, pp. 23658-23663, 2011. DOI: 10.1364/OE.19.023658

[6] D. J. Blumenthal, R. Heideman, D. Geuzebroek, A. Leinse, and C. Roeloffzen, “Silicon nitride in silicon photonics,” *Proceedings of the IEEE*, vol. 106, no. 12, pp. 2209-2231, 2018. DOI: 10.1109/JPROC.2018.2861576

[7] K. McNulty, M. V. Niekerk, V. Deenadayalan, C. E. Herranz, M. W. Pruessner, M. L. Fanto, and S. F. Preble, “Wafer scale fabrication of silicon nitride MEMS phase shifters with XeF2 dry vapor release etch process,” presented at *Silicon Photonics XVII (SPIE OPTO)*, San Francisco, United States, 2022. DOI: 10.1117/12.2606849

[8] J. Briere, M. Y. Elsayed, M. Saidani, M. Bérard, P. O. Beaulieu, H. Rabbani-Haghighi, F. Nabki, and M. Ménard, “Rotating circular micro-platform with integrated waveguides and latching arm for reconfigurable integrated optics,” *Micromachines*, vol. 8, no. 12, pp. 354, 2017. DOI: 10.3390/mi8120354

[9] S. Sharma, N. Kohli, J. Brière, F. Nabki, and M. Ménard, "Digitally Controlled Silicon Nitride Optical Switch," in *Optical Fiber Communication Conference (OFC)*, San Diego, United States, 2022. https://ieeexplore.ieee.org/document/9748541